Preliminary Evaluation of the Effective Diven Factor and Comparison with IPEN/MB-01 Measurement

YuGwon Jo[a]*, Jaeuk Im[a], Yunki Jo[a], and Sung Hoon Choi[a]
[a]Korea Atomic Energy Research Institute, 989-111 Daedeok-daero, Yuseong-gu, Daejeon, Korea, 34057
*Corresponding author: yugwonjo@kaeri.re.kr

***Keywords : Effective Diven Factor, Effective Delayed Neutron Fraction, IPEN/MB-01, PRAGMA**

1. Introduction

Neutron noise techniques such as the Feynman-α [1] and Cohn-α [2] methods infer the kinetics parameters of a zero-power reactor from the signal correlation induced by fission neutron multiplicity. The magnitude of this correlation is dictated by the second factorial moment of the multiplicity distribution, which is conventionally expressed through the Diven factor [3].

Since the standard point kinetics parameters are derived using the fundamental-mode adjoint flux, representing the fission importance, as a weighting function, the neutron noise model must share this weighting to maintain theoretical consistency. Consequently, the effective Diven factor, D_{eff}, was rigorously derived using the adjoint weighting function to account for both spatial, energy, and isotopic dependences [4].

Compared with the effective delayed neutron fraction, β_{eff}, and the prompt neutron generation time, Λ_{eff}, the calculation of D_{eff} has received relatively less attention. The present work preliminarily investigates two numerical weighting schemes to estimate D_{eff} using the GPU-based continuous-energy Monte Carlo code PRAGMA [5]. The first is a particle-based scheme that directly evaluates the second moment of importance via the iterated fission probability (IFP) [6] method to compute a weighted sum of the progenitor's tally. The second is a mesh-based scheme that suppresses the statistical bias inherent in the former by utilizing the adjoint flux and reaction rates tallied over a spatial mesh. To validate the two schemes, the IPEN/MB-01 benchmark [7] is examined to derive an experimental D_{eff} using an independently measured β_{eff}.

2. Effective Diven Factor

2.1. Definition in Neutron Noise Analysis

sadf

$$D = \frac{\overline{\nu(\nu-1)}}{\bar{\nu}^2}, \tag{1}$$

where the bar denotes the expectation over the multiplicity distribution. Since evaluated nuclear data libraries such as ENDF/B, JEFF, and JENDL tabulate only the first moment, the second factorial moments are derived from the prompt multiplicity measurements of Zucker and Holden [8].

To resolve inconsistencies in absolute multiplicity values between the measurements of Zucker and Holden and the underlying evaluated nuclear data libraries used for particle transport, these measurements are converted into the Diven factor, D_{ZH}, which is then combined with the tabulated first moment in the nuclear data libraries, $\bar{\nu}_{\text{LIB}}$, as:

$$\overline{\nu(\nu-1)} = D_{\text{ZH}}\bar{\nu}_{\text{LIB}}^2. \tag{2}$$

Table I summarizes the D_{ZH} values for U-235 and U-238 as a function of the incident neutron energy, E_n.

Table I. Diven factors of U-235 and U-238 evaluated by Zucker and Holden [8]

Nuclide	E_n (MeV)	$\bar{\nu}$	$\overline{\nu(\nu-1)}$	D_{ZH}
U-235	0	2.4140	4.6382	0.7959
	1	2.5237	5.1014	0.8010
	2	2.6368	5.6230	0.8087
	5	3.0387	7.6255	0.8258
	10	3.8750	12.4971	0.8323
U-238	0	2.2754	4.3406	0.8384
	1	2.4306	4.8960	0.8288
	2	2.5857	5.5152	0.8249
	5	3.0513	7.7066	0.8277
	10	3.8272	12.4099	0.8472

In a point reactor model, the auto power spectral density of the Langevin noise source is proportional to the fission rate and the Diven factor [3]. Extending the derivation to three-dimensional phase space and weighting the Langevin noise source by the adjoint importance yields [4]:

$$\Phi_{\text{SS}}(\omega) = 2R_{\text{f}}D_{\text{eff}}\bar{\nu}^2, \tag{3}$$

$$D_{\text{eff}} = \frac{R_{\text{f}}\int \mathrm{d}y R_{\text{f}}(y)\overline{\nu(\nu-1)}_y I^2(y)}{[\int \mathrm{d}y R_{\text{f}}(y)\bar{\nu}(y)I(y)]^2}, \tag{4}$$

where $R_{\text{f}}(y)$ is the fission rate density at the phase-space point y, $I(y)$ is the expected adjoint importance of a neutron born at y, and R_{f} is the total fission rate. For a spatially uniform importance, Eq. (4) reduces to the Diven factor of Eq. (1).

2.2. Derivation of Experimental Value

The IPEN/MB-01 benchmark [7] provides two independent measurements of β_{eff} utilizing different frequency regions of the power spectral density. The first one uses the cross power spectral density (CPSD) only in the plateau-region and the other is the broadband spectral fitting method. In the first method, the plateau-region CPSD relates the measured quantities to β_{eff} as:

$$\left(\beta_{\text{eff}}^{\text{plateau}}\right)^2 = D_{\text{legacy}}\left(\frac{2I_k I_m F_k F_m G_k G_m}{R_{\text{f}}\langle\Phi_{km}\rangle}\right)^{\text{exp}}, \tag{5}$$

where $\langle\Phi_{km}\rangle$ is the plateau level of the CPSD for the two different detectors k and m, while I, F, and G denote the detector current, the current-to-voltage conversion factor, and the filter-gain factor for the voltage signal, respectively. The superscript "exp" indicates that the entire bracketed term consists of experimentally measured quantities. To evaluate $\beta_{\text{eff}}^{\text{plateau}}$, D_{legacy} was set to 0.795, a value reported for U-235 in Ref. [3]. With this assumed value, $\beta_{\text{eff}}^{\text{plateau}}$ is obtained as 0.00739 ± 0.00007 [9].

The second method, employing the broadband spectral fit, reports an independent measurement for $\beta_{\text{eff}}^{\text{broad}}$ of 0.00750 ± 0.00019 [10]. Unlike the plateau method, this broadband fitting approach does not depend on an assumed Diven factor.

Because the experimentally measured bracketed term in Eq. (5) is a physical constant for the given reactor state, replacing $\beta_{\text{eff}}^{\text{plateau}}$ with the independently measured $\beta_{\text{eff}}^{\text{broad}}$ allows for the derivation of the experimental Diven factor as:

$$D_{\text{eff}}^{\text{exp}} = D_{\text{legacy}}\left(\frac{\beta_{\text{eff}}^{\text{broad}}}{\beta_{\text{eff}}^{\text{plateau}}}\right)^2. \tag{6}$$

Substituting the two β_{eff} values into Eq. (6) yields an experimental value of 0.819 ± 0.044, where the uncertainty, σ_D, is obtained as:

$$\sigma_D = D_{\text{eff}}^{\text{exp}}\sqrt{\left(2\frac{\sigma_{\beta,\text{broad}}}{\beta_{\text{eff}}^{\text{broad}}}\right)^2 + \left(2\frac{\sigma_{\beta,\text{plateau}}}{\beta_{\text{eff}}^{\text{plateau}}}\right)^2}, \tag{7}$$

where $\sigma_{\beta,\text{broad}}$ and $\sigma_{\beta,\text{plateau}}$ are the uncertainties in $\beta_{\text{eff}}^{\text{broad}}$ and $\beta_{\text{eff}}^{\text{plateau}}$, respectively.

3. Evaluation Methods

3.1. Particle-Based Scheme

The IFP method estimates the importance of an individual fission neutron from the number of its progenies after a specified number of latent cycles [6]. To apply this estimator to Eq. (4), we need the second moment of the fission importance. Since the importance of the individual fission neutron is affected by a large statistical error, substituting $I(y) = \bar{I}(y) + \sigma_I(y)$ into Eq. (4) and evaluating its expectation yields:

$$\begin{aligned} E\left[\widehat{D}_{\text{eff}}\right] &\approx \frac{R_f \int dy\, R_{\text{f}}(y)\overline{\nu(\nu-1)}_y\left(\bar{I}(y)+\sigma_I(y)\right)^2}{\left[\int dy\, R_{\text{f}}(y)\bar{\nu}(y)\bar{I}(y)\right]^2} \\ &= \bar{D}_{\text{eff}} + \frac{R_{\text{f}}\int \text{d}y R_{\text{f}}(y)\overline{\nu(\nu-1)}_y\sigma_I^2(y)}{\left[\int \text{d}y R_{\text{f}}(y)\bar{\nu}(y)\bar{I}(y)\right]^2} \end{aligned} \tag{8}$$

where $\bar{D}_{\text{eff}}$ is the true mean of the effective Diven factor,

$$\bar{D}_{\text{eff}} = \frac{R_{\text{f}}\int \text{d}y R_{\text{f}}(y)\overline{\nu(\nu-1)}_y\bar{I}^2(y)}{\left[\int \text{d}y R_{\text{f}}(y)\bar{\nu}(y)\bar{I}(y)\right]^2}, \tag{9}$$

and $\bar{I}(y)$ and $\sigma_I^2(y)$ are the mean and variance of the importance estimate.

As shown in Eq. (8), the bias is proportional to the variance of importance estimate. Furthermore, an increase in the latent cycles amplifies this variance, leading to the growth of the $\widehat{D}_{\text{eff}}$.

3.2. Mesh-Based Scheme

The variance of the importance of the individual particle cannot be controlled directly. To suppress the variance, the importance is accumulated on a spatial mesh. Using the mesh-wise tallies, D_{eff} can be evaluated as:

$$D_{\text{eff}} = \frac{R_f \sum_{i=1}^{N} R_{\overline{\nu(\nu-1)},i} I_i^2}{\left(\sum_{i=1}^{N} R_{\bar{\nu},i} I_i\right)^2}, \tag{10}$$

where N is the number of spatial meshes, i denotes the mesh index, and the mesh-wise tallies are defined as:

$$R_{\overline{\nu(\nu-1)},i} = \int_{y\in V_i} dy\, R_f(y)\overline{\nu(\nu-1)}\Big|_y \tag{11}$$

$$R_{\bar{\nu},i} = \int_{y\in V_i} dy\, R_f(y)\bar{\nu}(y), \tag{12}$$

$$I_i = \int_{y\in V_i} dy\, I(y). \tag{13}$$

4. Results and Discussion

The D_{eff} of the IPEN/MB-01 benchmark was estimated using the two different schemes implemented in PRAGMA. For the continuous-energy Monte Carlo calculation, 50 million histories per cycle were simulated with 50 inactive and 50 active cycles, utilizing the ENDF/B-VIII.1 [11] library. For the particle-based scheme, the sensitivity analysis was performed by varying the number of latent cycles to 1, 2, 4, 10, and 20. For the mesh-based scheme the spatial domain was discretized using a pin-wise radial mesh by varying the number of axial mesh divisions to 1, 5, 10, and 20, where the number of latent cycles for adjoint tally was fixed at 20.

Table II and Figure 1 show the calculated D_{eff} from the particle-based scheme as a function of latent cycles. As theoretically predicted, the positive bias grows rapidly with the number of latent cycles, causing the estimated values to severely diverge. Interestingly, the constant weighting approximation (denoted as 0 latent cycles), which ignores the spatial importance distribution, yielded a value of 0.798, showing the smallest deviation of –2.6% from the experimental value.

Table II. Calculated D_{eff} from particle-based scheme

Latent cycles	Mean	Std. Dev.	Deviation (C-E, %)
0[1]	0.798	0.0000002	−2.6
1	1.264	0.0000711	+54.3
2	1.701	0.0000994	+107.7
4	2.614	0.0001383	+219.2
10	5.451	0.0003876	+565.6
20	10.223	0.0009692	+1148.2

[1]Constant weighting is applied.

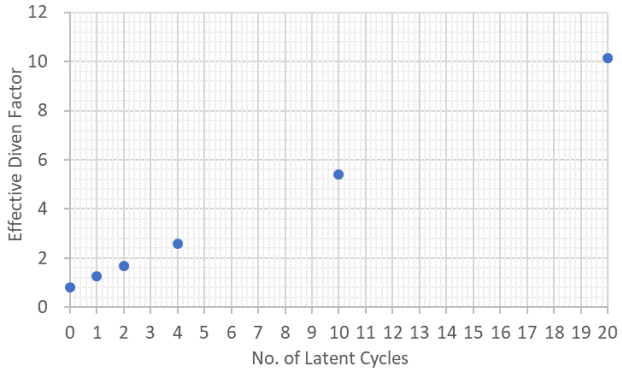


Figure 1. D_{eff} from particle-based scheme against the number of latent cycles.

Table III and Figure 2 show the calculated D_{eff} from the mesh-based scheme with respect to the number of axial mesh divisions. Unlike the particle-based approach, the mesh-based scheme successfully suppresses the variance-induced divergence, converging to 0.938 as the axial mesh becomes finer. However, this converged estimate overpredicts the experimental value by approximately 15%, which exceeds the 2-sigma range of the experimental uncertainty.

Table III. Calculated D_{eff} from mesh-based scheme

Axial divisions	Mesh size (cm)	Effective Diven factor (C)	C/E
1	54.84	0.8789	1.07 ± 0.06
5	10.97	0.9287	1.13 ± 0.06
10	5.48	0.9360	1.14 ± 0.06
20	2.74	0.9380	1.15 ± 0.06
Experiment (E)	–	0.819 ± 0.044	–

The statistical uncertainty of each calculated value is ± 0.0001.

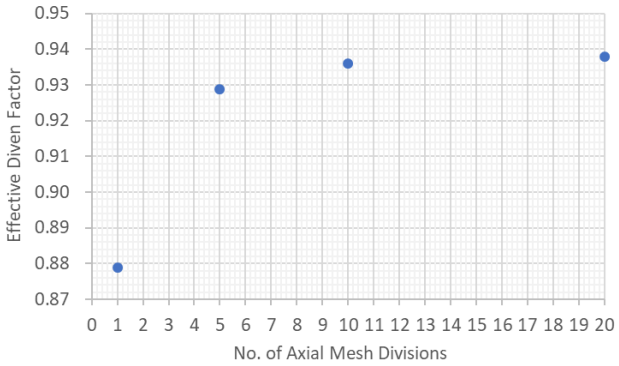


Figure 2. D_{eff} from mesh-based scheme against the axial mesh divisions.

5. Summary and Conclusions

Two numerical weighting schemes for the effective Diven factor were implemented in PRAGMA and compared with an experimental reference derived from the IPEN/MB-01 measurement. The particle-based scheme is severely biased by the variance of the individual importance estimate, causing the predicted values to diverge rapidly as the number of latent cycles increases. In contrast, the mesh-based scheme successfully suppresses this variance-induced divergence, converging to 0.938. However, this converged estimate still overpredicts the experimental reference by approximately 15%. Although the constant weighting approximation yields 0.798, which shows the smallest deviation from the reference, it remains physically inconsistent since it does not account for the spatial importance. A further work will investigate the origin of the 15% discrepancy in the mesh-based scheme and assess the effects of different nuclear data libraries on the D_{eff} estimation.

Acknowledgement

This work was supported by the National Research Foundation of Korea (NRF) grant funded by the Korea government (MSIT). (No. RS-2025-13222972).

REFERENCES

[1] R. P. Feynman, et al., "Dispersion of the neutron emission in U-235 fission", J. Nucl. Energy, vol. 3, pp. 64-69, 1956.
[2] C. E. Cohn, "A Simplified Theory of Pile Noise," Nucl. Sci. Eng., vol. 7, pp. 472-475, 1960.
[3] B. C. Diven, et al., "Multiplicities of Fission Neutrons," Phys. Rev., vol. 101, pp. 1012-1015, 1956.
[4] S. Okajima, et al., "A Note on the Diven Factor in Fast Systems," J. Nucl. Sci. Technol., vol. 37(8), pp. 720-723, 2000.
[5] N. Choi, K. M. Kim, and H. G. Joo, "Optimization of neutron tracking algorithms for GPU-based continuous energy Monte Carlo calculation," Ann. Nucl. Energy, vol. 162, 108508, 2021.
[6] B. C. Kiedrowski, F. B. Brown, and P. P. H. Wilson, "Adjoint-Weighted Tallies for k-Eigenvalue Calculations with Continuous-Energy Monte Carlo," Nucl. Sci. Eng., vol. 168, pp. 226-241, 2011.
[7] A. dos Santos, et al., "Reactor Physics Experiments in the IPEN/MB-01 Research Reactor Facility (IPEN(MB01)-LWR-RESR-001)," International Reactor Physics Experiment Evaluation Project, NEA/NSC/DOC(2006)1, Rev. 1, OECD-NEA, 2013.
[8] M. S. Zucker and N. E. Holden, "Neutron Multiplicity for Neutron Induced Fission of ^{235}U, ^{238}U, ^{239}Pu as a Function of Neutron Energy," BNL-38665 (IAEA-SM-293/122), Brookhaven National Laboratory, USA, 1986.
[9] A. dos Santos, et al., "A proposal of a benchmark for β_{eff}, β_{eff}/Λ, and Λ of thermal reactors fueled with slightly enriched uranium," Ann. Nucl. Energy, vol. 33, pp. 848-855, 2006.
[10] R. Diniz, and A. d. Santos, "Experimental Determination of the Decay Constants and Abundances of Delayed Neutrons by Means of Reactor Noise Analysis", Nucl. Sci. Eng., vol. 152, pp. 125-142, 2006.
[11] G. P. A. Nobre, et al., "ENDF/B-VIII.1: Updated Nuclear Reaction Data Library for Science and Applications," Nucl. Data Sheets, vol. 210, pp. 1-224, 2026.